Desalination and Water Treatment
www.deswater.com

doi: 10.5004/dwt.2020.25601

187 (2020) 410–426
May

Simultaneous removal of binary cationic dyes from wastewater by nanoscale zero-valent iron particles supported on multi-walled carbon nanotubes/attapulgite

Yajuan Zhang, Hui Xu*, Jin Tang, Lei Tian, Minzhang Chen, Weiguo Tian, Guojun Gou, Yong Chen*

College of Petrochemical Technology, Lanzhou University of Technology, Lanzhou, China, Tel. +86-931-2975872; emails: xuhui@lut.cn (H. Xu), chenylut@126.com (Y. Chen)

Received 19 September 2019; Accepted 19 January 2020

ABSTRACT

In the paper, the study involves the development of novel recyclable multi-walled carbon nanotubes/attapulgite supported nanoscale zero-valent iron (nZVI/MWCNTs/APT) composites and used for the removal cationic dyes methylene blue (MB) and malachite green (MG) in binary systems. The morphology and structure of ternary nanocomposites were characterized by using different techniques like transmission electron microscopy, X-ray diffraction, Fourier-transform infrared spectroscopy, Brunauer–Emmett–Teller, and ZETA. And remove performances for MB and MG were investigated in detail. The experimental results revealed that the dispersion and stability of nZVI were significantly improved by MWCNTs/APT composite as a supporter. Compared to bare nZVI, the nZVI/MWCNTs/APT exhibited much higher removal efficiency on MB and MG due to the good synergistic effect between MWCNT/APT adsorption and nZVI reduction. The removal efficiencies of MB and MG in the nZVI/MWCNTs/APT system were 97.9% and 98.9% after reacting for 90 min, respectively. The kinetics and isotherm studies for MG and MB degradation by nZVI/MWCNTs/APT system could be well described by the pseudo-second-order kinetic model and Langmuir adsorption isotherm model. The maximum adsorption capacities of MB and MG reached to 149.9 and 177.9 mg/g, respectively, which showed higher adsorption performances compared to the other adsorbents. The possible removal mechanism and degraded intermediates of MG and MB were proposed by using gas chromatograph–mass spectrometry analysis and UV-vis spectrum techniques. More importantly, the spent adsorbent has a certain specific capacitance and can be used as electrode materials in supercapacitors, which provides a basis for the recycling of discarded materials. The present investigation concluded that nZVI/MWCNTs/APT nanocomposites might be a suitable and cost-effective alternative for the removal of organic dyes in wastewater.

Keywords: Nanometer zero-valent iron; Multi-walled carbon nanotubes; Attapulgite; Cationic dyes; GC-MS analyzing

1. Introduction

In the past few decades, with the rapid development of technology and business, the dye preparation technology was more complete and the variety was more numerous. The total number of dye, including natural and synthetic, is up to million tons that were extensively applied to textile, printing, paint, and pigment [1,2]. The process of dye application will generate large amounts of waste effluents, which directly discharge into natural water resources that caused severe water pollution problems. The organic dyes contain

* Corresponding authors.

various toxic chemical groups such as benzene rings, anthracene rings, etc., which have diverse harmful effects on aquatic and public life. Methylene blue (MB) and Malachite green (MG) are cationic dyes and customarily used stuff in various industries. Due to the complex aromatic molecular structures that make them have more potential carcinogenic and mutagenic risk and must be cautiously used. Mu Naushad's research group carried out a large amount of research different materials to remove MB and MG within single system [3,4]. However, the actual wastewater has multiple components of dye and competitive adsorption occurs in various dyes coexist systems to result in the decreased removal of dyes. Thus, the simultaneous removal of multiple organic dyes from wastewater has an especial significance to both pollution control and environmental remediation. Many methods have been developed, including membrane separation, ion exchange method, photodegradation, adsorption, and others [5–7]. Among these methods, reactions incorporating catalytic materials degradation pollutants are becoming a more ideal path for organic contaminants, which will degrade contaminants to completely harmless final products. Redox degradation has enormous potential for the removal of aqueous pollutants.

In the last decade, nanoscale zero-valent iron (nZVI) has attracted great attention for the removal of heavy metal ions and organic pollutants from wastewater due to its high activity, large surface area, and low cost [8]. The nZVI is a strong reducing agent and can be used for the removal of a serious of contaminants to involve in various removal mechanisms, such as reduction, adsorption, and even oxidation through the Fenton mechanism [9]. The research results indicated that the main mechanism of the system containing nZVI was reductive degradation to damage dyes' chromophore groups and conjugated systems [10]. However, the system of nZVI is easy to agglomerate and hinders its reduction rate due to the high surface energy. Besides, the high reactivity of nZVI particles can easily react with oxygen its surrounding media, resulting in the formation of an oxidation layer on the nZVI particle surface to inhibit the effective surface area and active sites [11]. These drawbacks severely limit the application of nZVI materials in real work to remediate the environmental. To solve these deficiencies some supporting materials were introduced to improve the dispersion and stability, for instance, kaolinite, bentonite, polyaniline, carbon, and metal-organic framework [12,13]. Natural clays (such as kaolin, zeolite, and montmorillonite) with porous structure and high surface area were usually evaluated as support material for nZVI. The abundant natural resources attapulgite (APT) owned unique one-dimensional structures, high surface specific area and environmental stability were considered as suitable support materials [14,15]. Despite APT has many advantages, it still suffers from poor adsorption capacity and difficult to reuse. A feasible solution is to use a stable substrate with abundant active sites to combine clay nanomaterial to increase its adsorption efficiency [16,17].

Carbon nanotubes (CNTs) also have been used as versatile matrices to disperse metal nanoparticles to fabricate high-performance nanocomposites to exert synergistic effect of individual components properties [18]. The hollow tubular structure of CNTs could not only provide a large specific surface area but also possesses a large number of oxygen-containing functional groups such as hydroxyl (–OH), carboxyl (–COOH), carbonyl (–C=O), that can form a strong adsorption for contaminant by chemical bonding [19,20]. CNTs as adsorbent materials can provide a good prospect of applications for removing dyes from aqueous solutions. Hence, the great combination of CNTs and APT to form composite supporter is an effective approach to improve the dispersion and stability of nZVI synergistically.

In this work, multi-walled carbon nanotubes/attapulgite (MWCNTs/APT) composite supporter was introduced into the nZVI system to remove cationic dyes of MB and MG in binary systems. The wastewater generally contains multiple components and affects dye removal behavior. As per the best of our knowledge, few studies have been reported to remove MB and MG by nZVI/MWCNTs/APT in binary systems. Therefore, it is important to study new efficient nZVI composites for dyes removal of multiple dyes system. The aims at this study were to (1) investigate the removal performance of both cationic dyes and other dyes by nZVI/MWCNTs/APT nanocomposite; (2) elucidate the various factors affecting to the removal MB and MG; (3) characterize microstructure and surface features of nZVI/MWCNTs/APT before and after reaction to dyes; (4) illuminate the kinetics adsorption isotherm model and thermodynamics for MG and MB degradation and propose reasonable removal mechanism of dyes; (5) investigate the recycling of the spent adsorbent.

2. Experimental details

2.1. Reagents and chemicals

Attapulgite (99%, APT) (JC-J503) was purchased from Jiangsu Xuyi Nanomaterial Science and Technology Co. Ltd., China analytical reagent grade ferrous sulfate heptahydrate ($FeSO_4{\cdot}7H_2O$), sodium borohydride ($NaBH_4$) were purchased from Tianjin Kaixin Chemical Reagent Co. Ltd., China. MWCNTs (diameter of 4–6 nm, length of 10–20 lm, purity > 98 wt.%) were purchased from Chengdu Organic Institute, China. Hydrochloric acid (HCl), sodium hydroxide (NaOH), and hexadecyl trimethyl ammonium bromide (CTAB) was analytical grade reagent. MB, MG, Naphthol Green B (NGB), Methyl Orange (MO), Alizarin Yellow R (AYR), Orange IV, Crystal Violet (CV), Basic Fuchsin (BF), Rhodamine B (RhB), etc. were offered by Shanghai Zhongtai Chemical Reagent Co. Ltd., China.

2.2. Synthesis of nZVI and nZVI/MWCNTs/APT

APT pretreatment: 0.656 g CTAB (CTAB is an abbreviation for cetyltrimethylammonium bromide. The chemical formula is $C_{16}H_{33}$ $(CH_3)_3NBr$) was introduced into 100 mL 100 g/L APT suspension under electromagnetic stirring for 12 h. The solid was filtered, washed and then dried in a vacuum at 60°C for 24 h to obtain the modified APT.

MWCNTs/APT supported nZVI composite sample was prepared to use a liquid-phase reduction method. 0.5 g modified APT and 0.25 g $FeSO_4{\cdot}7H_2O$ were added into a 250 mL three-necked flask that was scattered with stirred and ultrasound for 10 min. That 0.1 g MWCNTs were added

into 50 mL deionized water was dispersed by ultrasonic 40 min, which was transferred into above the mixture solution to three-neck flask, 0.076 g $NaBH_4$ (dissolved in 100 mL deionized water) was added dropwise (with 300 rpm) with stirring. The solid material was filtered and washed with distilled water and alcohol repeatedly. The resulting nZVI/MWCNTs/APT composite was dried in a vacuum oven at 60°C. The entire reduction experiment was carried out under the protection of nitrogen.

Bare nZVI nanoparticles were directly prepared for dropping $NaBH_4$ into $FeSO_4{\cdot}7H_2O$ aqueous solution.

2.3. Characterizations and measurements

Fourier transforms infrared concerning composite materials were obtained employing Fourier-transform infrared spectroscopy (FT-IR, NEXQS670, America) using KBr pellets. Morphology and structure of composite materials were observed by a transmission electron microscope (TEM, JEM-1200EX, America). X-ray diffraction patterns were collected on an X-ray diffractometer (XRD, D/MAX–2400X, Japan) using Cu Kα radiation (λ = 0.15406 Å) in a 2θ range of 10°–90° at room temperature. Spectrophotometry was used for the measurement of the concentration of dyes in solution at specific adsorption wave on a 7230G spectrophotometer (Shanghai Precision Scientific Instrument Co. Ltd., China), The N_2 adsorption–desorption, specific surface area and pore size distribution of the sample were analyzed by American ASAP 2020 plus HD88 specific surface area and porosity analyzer, using the Barrett–Joyner–Halenda method, respectively. The pH measurements were conducted with a glass electrode (PHS-3D Model pH meter, China). Zeta potential (Malvern Instrument Zetasizer Nano-ZS) was obtained at room temperature.

2.4. Batch adsorption experiments

Adsorption experiments of MB and MG on nZVI/MWCNTs/APT in binary dye systems with 500 rpm for 90 min at 298 K were carried out in a batch mode. The effects of various influence factors were studied in binary dye systems, including the influence of variable pH (2–12), mixed solutions concentration (25–50 mg/L) and dose of the adsorbents (20–100 mg). The solution pH was adjusted to the desired value by the negligible amount of HCl and NaOH. They were then filtered through 0.45 μm membranes to measure the residual concentration of dye. The concentration of dye was measured using UV-Spectrophotometer. The removal capacity (q_B) and the removal efficiency (R) of dye were calculated using the following Eqs. (1) and (2):

$$q_B = \frac{C_0 - C_e}{m} \times V \tag{1}$$

$$R = \frac{C_0 - C_e}{C_0} \times 100\% \tag{2}$$

where C_0 and C_e are the initial and equilibrium concentrations of dye in solution (mg/L), V is the volume of solution (L), m is the mass of adsorbent (g).

2.5. Determination of the concentration of two-component dyes

In general, the absorbance and absorption values were determined at their λ_{max} of a single system, but for two-component dyes, where is a large spectral interference in the spectrum. There may be caused inexact to obtain absorbance value at a single dye's λ_{max} and calculate the residual concentration of the dye by using a standard curve. The simultaneous solution of the equations will solve the question of spectral overlapping. In binary dye systems, the concentration of dye was measured using a UV-Spectrophotometer (7230G, China) at two wavelengths of 664 and 617 nm. The dye concentrations of solutions were determined by the following Eqs. (3) and (4) [21]:

$$C_{MB} = \frac{k_{B2}A_1 - k_{B1}A_2}{k_{A1}k_{B2} - k_{A2}k_{B1}} \tag{3}$$

$$C_{MG} = \frac{k_{A1}A_2 - k_{A2}A_1}{k_{A1}k_{B2} - k_{A2}k_{B1}} \tag{4}$$

where C_{MB} and C_{MG} are the concentrations of components MB and MG in solution; k_{A1}, k_{A2}, k_{B1}, and k_{B2} are the calibration constants for components MB and MG at wavelength 664 and 617 nm, respectively, A_1 and A_2 are the absorbance at wavelength 664 and 617 nm.

2.6. Gas chromatograph–mass spectrometry analysis (GC–MS) for degradation products of MB and MG

Further identified through the Gas chromatograph–mass spectrometry analysis (GC/MS) analysis as the protocol described by [22] with minor alterations. The GC/MS system by America consists of an Agilent 6890GC equipped with an Agilent 5973 N mass selective detector (GC/MS) was used to detect the degradation products of MB and MG. The mass spectrometer was operated in the electron impact mode with an electron current of 70 eV. Aliquots of 1 μL were injected automatically with an autosampler (AUC20i) in splitless mode via a GC inlet. An HP-5 MS capillary column (30 m × 0.25 mm ID, 0.25 μm film thickness) was connected directly to the ion source of the mass spectrometer. The oven temperature was kept isothermal for 1 min at 50°C, was then increased to 270°C at a rate of 10°C min^{-1} and held at 270°C for 23 min. The injector, MS source, and MS quad temperature were 250°C, 230°C, and 150°C, respectively. The GC/MS system was operated in a full scan (m/z15–500). Controls and samples were analyzed in duplicate.

3. Results and discussion

3.1. Characterization of methods

The FT-IR spectrums of MWCNTs, APT, nZVI/MWCNTs/APT before and after reaction with dyes of MB and MG are shown in Fig. 1a. The FT-IR spectrum of the MWCNTs consisted of –OH (3,454 cm^{-1}), vibration peak (2,948 and 2,857 cm^{-1}) were related of the $–CH_2–$ groups, at the peak of 1,631 and 1,132 cm^{-1} was –C=O and –C–O, respectively [23]. And the peaks appearing at 3,454; 2,948; 2,857; 1,631; and 1,037 cm^{-1} were attributed to the bending and stretching

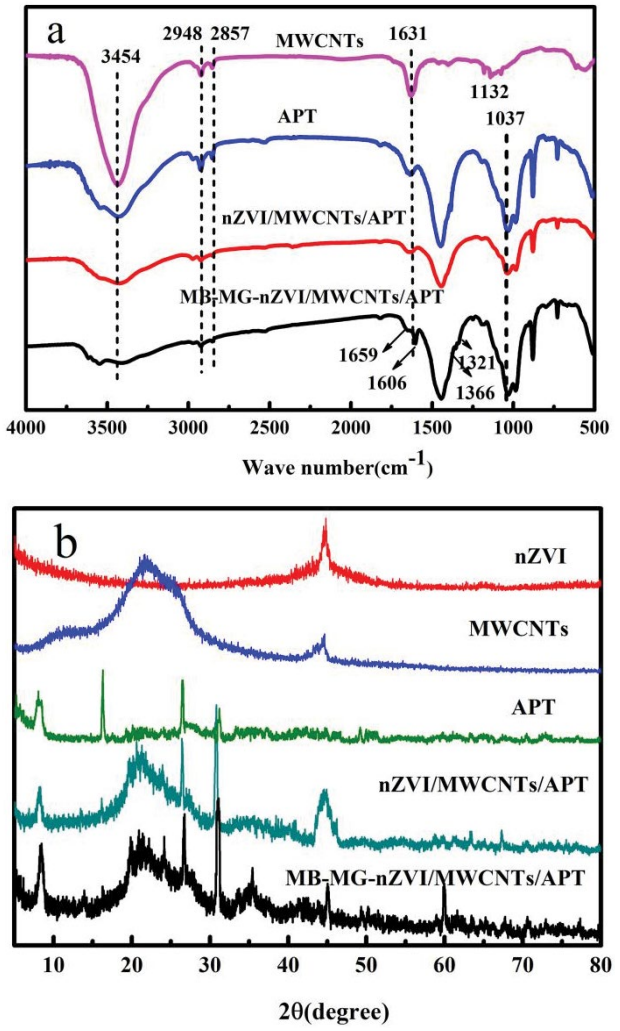

Fig. 1. (a) FT-IR image and (b) XRD patterns of MWCNTs, nZVI, nZVI/MWCNTs/APT before reaction and after reaction with dyes of MB and MG.

vibrations of APT [24,25]. The curve of composites contains both the peaks of MWCNTs and APT, illustrating the successful synthesis of composites nZVI/MWCNTs/APT. After the reaction to MB and MG, some weak peaks were appearing at 1,321 and 1,366 cm^{-1}, which belong to the symmetric vibration of $–CH_3$ and the ring stretch of MB [21], the peaks at 1,606 cm^{-1} corresponds to –C=C– the ring of MG [26], which showed the phenomenon adsorption MB and MG on nZVI/MWCNTs/APT. Obviously, the peaks of –OH at 3,454 cm^{-1} and –COOH at 1,631 cm^{-1} have a mild move to low wavenumber, indicating these groups affect the removal of the MG and MB.

The XRD patterns of nZVI, MWCNTs, nZVI/MWCNTs/APT before and after reaction with dyes of MB and MG were shown in Fig. 1b. The diffraction peak at 2θ = 44.8° is characteristic of nZVI, illustrating the iron in the sample is in the zero-valent state. The diffraction peak at 2θ = 21.9° and 2θ = 44.6° assigned to MWCNTs, declaring the skeleton of the carbon tube is regular [27]. The diffraction peaks at 2θ = 8°, 20.7°, 26.4°, and 31° are the crystal structure of the APT [28]. Meanwhile, the diffraction characteristic peaks of nZVI and MWCNTs appear in the composites, indicating that APT, MWCNTs and nZVI maintain their respective complete skeleton that consistent with the analytical structure in the FT-IR. There are some changes in the XRD patterns of nZVI/MWCNTs/APT after reaction with dyes. The peak intensity of the Fe° was weakened attributed to the consumption and some new peaks appeared at 2θ = 24.3°, 35.4°, and 60.1° that represented Fe_2O_3 (hematite), Fe_3O_4 (magnetite), and Fe-OOH (goethite) [29]. It implies that some of Fe^0 is converted to Fe^{2+} and Fe^{3+} due to the oxidation reaction during the degradation of MB and MG.

The structure of the adsorbent largely affects the adsorption performance. In order to better analyze the dispersion of nZVI on the precursor MWCNTs/APT, the morphology of MWCNTs, nZVI, and the nZVI/MWCNTs/APT reaction before and after of dyes was investigated by TEM. From Fig. 2a it can be seen MWCNTs have a distinct tubular structure and smooth surface. As shown in Fig. 2b, the pure nZVI particles agglomerated to form chain-like structures, which mainly caused by magnetic interactions among iron particles. After combining with MWCNTs/APT composites, the slight aggregation of nZVI particles are still observed in Fig. 2c, but greatly lessened compared to the unsupported nZVI nanoparticles, which further to afford strong evidence to illustrate the removal efficiency of MWCNTs/APT supported nZVI becomes higher than bare nZVI. After reaction (Fig. 2d), the number of nZVI obviously decreased to imply that nZVI participate reaction.

The N_2 adsorption–desorption isotherms pore size distributions as Fig. S1 and the relevant data are shown in Table 1. The adsorption–desorption isotherm of nZVI/MWCNTs/APT belongs to type IV in the International Union of Pure and Applied Chemistry (IUPAC), hysteresis loop (H_3 type) appears in the region of relative pressure (0.75–0.95), indicating the presence of a certain meso/macroporous is beneficial to the adsorption of dye macro-molecules [30]. S_{BET} (BET – Brunauer–Emmett–Teller) of nZVI, nZVI/APT and nZVI/MWCNTs/APT are 17.51, 54.2 and 114.98 m^2/g, respectively. In contrast with nZVI and nZVI/APT, S_{BET} of nZVI/MWCNTs/APT is much larger than them. At the same time, the pore volume of nZVI/MWCNTs/APT is also much higher than that of nZVI and nZVI/APT. The results indicate that MWCNTs/APT as a carrier can effectively minimize nZVI agglomeration and increase the surface area, all these traits will benefit the removal of dyes.

3.2. Effect of different materials on dyes removal

To evaluate the different materials (nZVI, APT, nZVI/APT, and nZVI/MWCNTs/APT) degradation of MB and MG in the initial concentration of dyes 100 mL 50 mg L^{-1} to study the removal performances after reaction 90 min are investigated in Fig. 3. The results indicate the removal efficiency of nZVI and APT for MB and MG are about 44.9%, 79.5% and 55.3%, 84.7%, which is lower than composites nZVI/APT. This is attributed to the decreased reactivity of bare iron particles and the poor adsorption performance of APT. The removal efficiency of nZVI/MWCNTs/APT is higher than other materials, which can reach to 97.9% of MB and 98.9% of MG, respectively. An obvious growth proves that

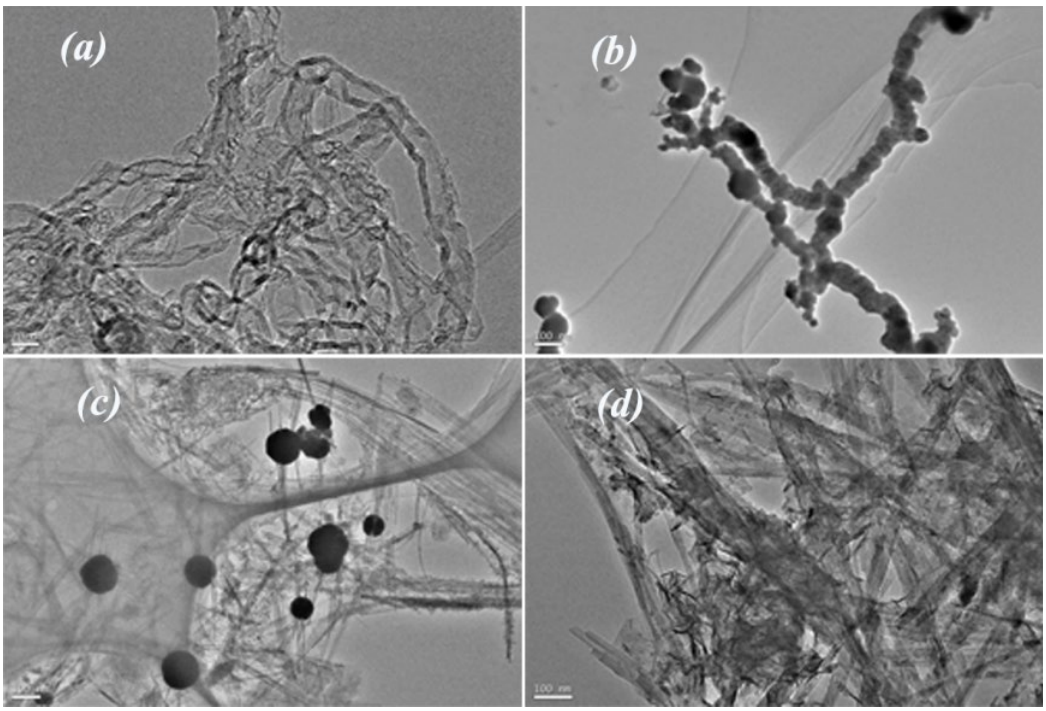

Fig. 2. TEM images of (a) MWCNTs, (b) nZVI, (c) nZVI/MWCNTs/APT before reaction, and (d) nZVI/MWCNTs/APT after reaction with dyes of MB and MG.

Table 1
BET data of the samples

Samples	S_{BET} (m^2/g)	V (m^3/g)	D (nm)
nZVI	17.51	0.045	10.39
nZVI/APT	54.20	0.132	9.76
nZVI/MWCNTs/APT	114.98	0.254	8.82

the removal ability of nZVI is more effective after supported by MWCNTs/APT. The MWCNTs/APT not only served as an adsorbent for dyes but also as a dispersant for nZVI, which enhanced the adsorption and catalytic reduction of MB and MG. Consequently, the high removal performance of nZVI/MWCNTs/APT was caused by the synergistic effect of the material.

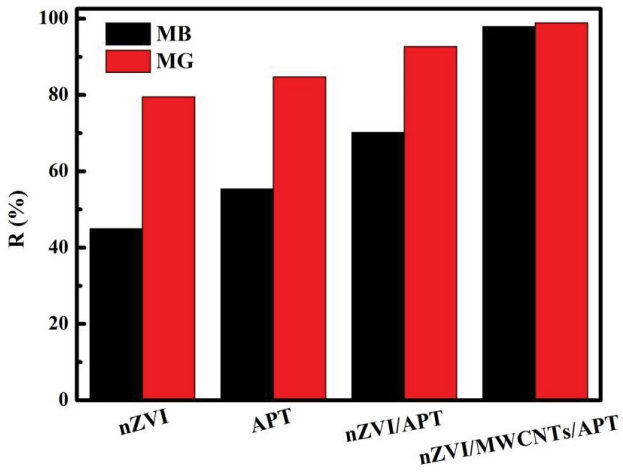

Fig. 3. Removal of MB and MG in binary systems using different materials.

3.3. Factors affecting the removal of MB and MG

3.3.1. Effect of pH in binary-dye solutions

The initial value pH of solution not only has a crucial effect on the color of dye in water but also is one of the most important factors that effect on removal property of composite materials [31]. The impact pH range of 2–12 to remove MB and MG using nZVI/MWCNTs/APT at different time intervals (0–90 min) is shown in Fig. 4a. It can be seen the removal efficiencies of MB and MG keep above 85% in the range of pH 4–12 and demonstrating alkalinity and the weak acid condition is beneficial to remove MB and MG. The possible reason is that the surface of the nZVI/MWCNTs/APT contains a large number of hydroxyls (–OH) and carboxyl groups (–COOH), which make the adsorbent negatively charged with alkaline medium and tend to adsorb with positively charged molecules, this result can be verified by zeta measurement. Fig. 4b shows nZVI/MWCNTs/APT with the negatively charged surface at the pH from 4 to 12, indicating the nZVI/MWCNTs/APT is more likely to adsorb cationic dyes by electrostatic attraction. This explained the reason that the removal efficiency increased under the strongly alkaline conditions with the sustained growth of pH. In strongly acidic solutions, since the adsorbent possesses positively charged surface come into being electrostatic repulsion between cationic dyes and adsorbent results

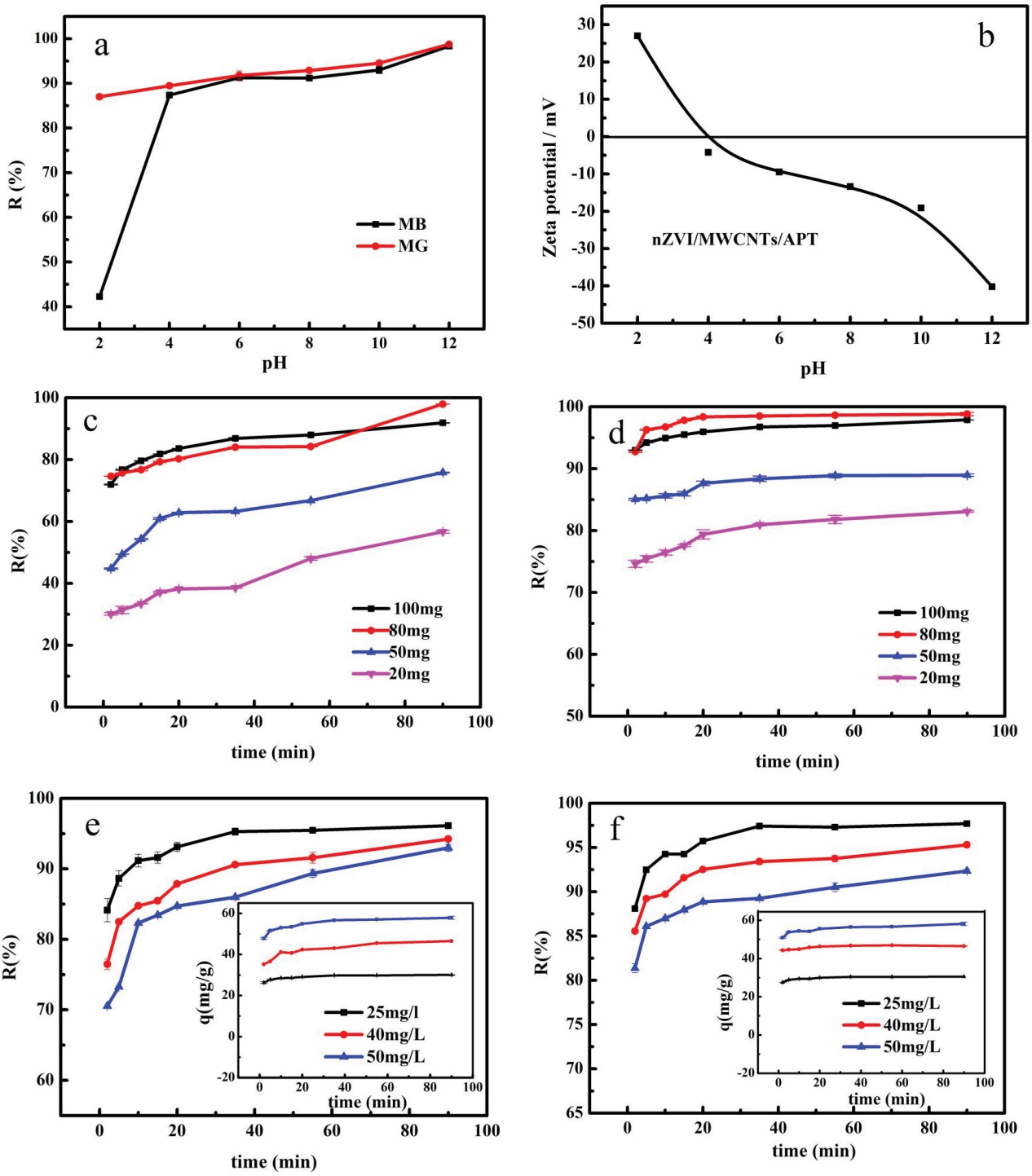

Fig. 4. (a) Effect of pH on removal of MB and MG in binary systems, (b) Zeta potential of nZVI/MWCNTs/APT as a function of solution pH, (c and d) effect of dosage on removal of MB and MG, (e and f) effect of dyes concentration on the removal of MB and MG in binary systems.

from the decreased removal efficiencies of MB (42.5%) and MG (86.9%). Furthermore, the lower of the removal rate of MB may be attributed to the more positive charges carried by the dye itself. It can be concluded that electrostatic attraction plays a crucial role in the removal of the dyes. Besides, hydrogen-bond and π–π stacking between dyes and adsorbents further enhanced the removal efficiency. The dye removal mainly depended on the adsorption and reduction process by nZVI/MWCNTs/APT nanocomposites. For the reduction and degradation of dyes, acidic conditions

are generally beneficial to improving the reactivity of nZVI that enhance the removal efficiencies of dyes in the reaction process, but this study results indicated that the neutral or alkaline conditions more facilitated the decolorization reaction than the acidic ones. The contradictory consequences inferred the high removal efficiencies were mainly attributed to the adsorption process by electrostatic, hydrogen bonding and π–π interactions.

3.3.2. Effect of dosages of nZVI/MWCNTs/APT in binary-dye solutions

The effect of adsorbent dosages (20–100 mg) on the removal efficiency at different time intervals (0–90 min) was studied in this experiment. As shown in Figs. 4c and d, with the amount of adsorbent change from 20 to 80 mg, the removal percentage of MB and MG ascend gradually from 56.68%, 83.06% to 97.94%, and 98.82%, respectively. This is because the specific surface area and active sites become more and more along with the amount of adsorbent increased [32]. However, the removal rate of binary dyes goes down when the adsorbent dosage was added up to 100 mg that may be attributed to overlapping or aggregation of adsorbent resulting in a decrease in the available surface area and an increase in diffusion path length [33]. According to the above analysis, the dosage of nZVI/MWCNTs/APT in this study has adopted 80 mg for the following experiments.

3.3.3. Effect of initial concentration of MB and MG

Initial concentration is one of the important criteria of dye adsorption, which is mainly by preparing a fixed amount of adsorbent and reacting to different initial concentrations of dye until equilibrium [34]. Also, the initial concentration provides an important driving force to overcome all mass transfer resistance of all molecules between the aqueous and solid phases [35]. That offers the basis of analyzing the reaction mechanism between adsorbent and dye. Figs. 4e and f shows the effect of initial concentration between 25 and 50 mg/L on removal efficiency by using nZVI/MWCNTs/APT. The removal efficiencies decrease as the initial concentration increases. When the concentration is 25 mg/L, the removal efficiencies of MB and MG are 96.2% and 97.5%, respectively. At 50 mg/L, the removal efficiencies drop to 92.8% and 93.1%. When the amount of adsorbent is constant the adsorption sites and specific surface area keep fixed. As the initial concentration increases, the adsorption site gradually becomes saturated to result in the removal rate of a decrease. Meanwhile, nZVI is rapidly oxidized to Fe(II) and Fe(III) when MB and MG are close to the nZVI/MWCNTs/APT surface to reduce the reactivity of composite [36]. However, with the concentration increases the mass transfer force increases between the adsorbent and the dye to increase the adsorption capacity. Take into account the removal efficiency, the concentration of the blended dye are adopted 50 mg/L.

3.4. Kinetic study

To perform the adsorption kinetics, 100 mL of a mixed solution of initial concentration (50–70 mg/L) was treated with 80 mg of nZVI/MWCNTs/APT at a fixed pH for the contact time 0–90 min at 298 K. Kinetic studies are critical to understanding the adsorption process because it provides information on the mechanism for adsorption rate and rate control [37]. This allows us to determine the equilibrium time required for the reaction and calculated the equilibrium constant of adsorption [38]. Fig. 5 shows the variation in adsorption capacity of different concentrations on time. It displays that adsorption occurred in three stages: (1) external surface fast adsorption, (2) slow adsorption, (3) adsorption equilibrium. Specifically, the first 5 min belongs to the fast adsorption stage, which the dye's molecule freely and fast attached to available active sites of the adsorbent. The slow adsorption stage is t = 35 min for MB and t = 55 min for the MG that the active sites are being gradually filled up as adsorption progressed. Subsequently, the effective adsorption site has reached saturation so the adsorption capacity will no longer improve as the adsorption time increased.

The kinetic models mainly include the pseudo-first-order (PFO), the pseudo-second-order (PSO), intraparticle diffusion (ID) and Elovich were applied to analyze the experimental data. The linearized forms of the equations are respectively expressed by using Eqs. (5)–(8):

$$\ln\left(q_e - q_t\right) = \ln q_e - k_1 t \tag{5}$$

$$\frac{t}{q_t} = \frac{t}{k_2 q_e^2} + \frac{t}{q_e} \tag{6}$$

$$q_t = k_p \sqrt{t} + C \tag{7}$$

$$q_t = \frac{1}{\beta}\ln\left(\alpha\beta\right) + \frac{1}{\beta}\ln t \tag{8}$$

where k_1 (min^{-1}) is the rate constant of PFO model adsorption, k_2 (g (mg min)$^{-1}$) is the rate constant of PSO model adsorption, q_e (mg/g) is the adsorption capacity at equilibrium, q_t (mg/g) is the adsorption capacity at time t, t (min) is contact time, k_p (mg·(g min$^{1/2}$)$^{-1}$)is the rate constant of intra-particle diffusion kinetic models and C is constant, which α (mg/g min^{-1}) and β (g/mg) is determined from the slope and intercept of the plot. The values of kinetic parameters are listed in Table 2.

As shown in Table 2 that R^2 values for the PSO kinetic model were greater than 0.99 ($R^2 > 0.99$) for MB and MG, whereas the R^2 of PFO, ID, Elovich kinetic model were less than 0.99 ($R^2 < 0.99$). The result demonstrates the adsorption processes are following the PSO kinetic model. Thus, it could be shown that the chemisorption is mainly the rate-limiting step that controls the MB and MG adsorption.

3.5. Adsorption thermodynamics study

3.5.1. Adsorption isotherm

Further to reveal the interaction between dyes and composite materials, the relationship between adsorption equilibrium concentration and adsorption capacity at different temperatures (303–323 K) and different concentrations (50–150 mg/L) was studied. The data onto adsorption

Table 2
Adsorption kinetics parameters of in binary-dye solutions

Model	Parameters	MB adsorption C_0 (mg/L)			MG adsorption C_0 (mg/L)		
		50	60	70	50	60	70
PFO	k_1	0.0462	0.0823	0.0751	0.0414	0.0880	0.0658
	q_e	1.4319	3.7984	3.1224	0.9825	8.1754	6.3096
	R^2	0.7064	0.9685	0.9122	0.6139	0.9927	0.9324
PSO	k_2	0.0904	0.0327	0.0633	0.1212	0.0282	0.0265
	q_e	61.54	73.86	85.11	62.38	74.79	86.51
	R^2	1	0.9952	0.9952	1	0.9999	0.9999
ID	k_p	0.2402	0.3591	0.2528	0.1537	0.6789	0.5344
	C	59.53	70.64	82.87	61.05	68.96	81.55
	R^2	0.4381	0.6437	0.7935	0.5326	0.6816	0.8912
Elovich	A	7.9×10^{35}	5.0×10^{29}	4.4×10^{52}	8.9×10^{59}	2.9×10^{15}	1.5×10^{25}
	B	1.4167	0.9856	1.4812	2.2954	0.5250	0.7201
	R^2	0.6488	0.8374	0.8915	0.7064	0.8694	0.9352

equilibrium has been analyzed using the well-known Langmuir, Freundlich and Temkin models. The Eqs. (9)–(11) are as follows:

$$\frac{C_e}{q_e} = \frac{C_e}{q_m} + \frac{1}{q_m b} \tag{9}$$

$$\ln q_e = \ln k_F + \frac{1}{n} \ln C_e \tag{10}$$

$$q_e = \beta \ln k_T + \beta \ln C_e \tag{11}$$

where q_m (mg/g) is the calculated adsorption capacity at maximum, q_e (mg/g) is the experimental adsorption capacity at equilibrium, C_e (mg/L) is the equilibrium concentration of the solution, k_L (L/mg) is a Langmuir constant, k_F (mg/L) is a Freundlich constant, $\beta = RT/b$, T is the absolute temperature in Kelvin, R the universal gas constant (8.314 J K^{-1} mol^{-1}), k_T the equilibrium binding constant, and the constant β is related to the heat of adsorption.

The fitting result of experimental data was recorded in Table 3. At the same time, this studied further compares the standard deviation (SD) of the above model fitting parameters considering the accuracy problem [39]. The smaller the SD value, the higher the accuracy of the model.

From the parameters, correlation coefficients and SD of the isothermal model listed in Table 3 to conclude that both MB and MG were following the Langmuir isotherm model belongs to the monolayer adsorption. The maximum adsorption capacity of MB and MG increases as the temperature elevate, indicating that the thermal vibration has a greater impact on the adsorption process [40]. The maximum adsorption capacities of MB and MG were 149.9 and 177.9 mg/g, respectively. Besides, Table 4 summarizes the maximum adsorption capacity of various adsorbents has been reported to removing MB and MG. It is worth noting that the composite nZVI/MWCNTs/APT of this study has higher adsorption capacity and shorter equilibrium time. Therefore, nZVI/MWCNTs/APT composites will be a promising material for treatment binary dyes from wastewater.

3.5.2. Thermodynamic parameter

Thermodynamic data can reflect the feasibility of adsorption, which can reflect the effect of temperature on adsorption and the data analysis is shown in Table 5. Thermodynamic parameters are free energy change ($\Delta G°$), enthalpy change ($\Delta H°$) and entropy change ($\Delta S°$) to calculate by the following Eqs. (12)–(14):

$$K_d = \frac{q_e}{C_e} \tag{12}$$

$$\Delta G° = -RT \ln K_d \tag{13}$$

$$\ln K_d = \frac{\Delta S°}{R} - \frac{\Delta H°}{RT} \tag{14}$$

where q_e (mg/g) is the experimental adsorption capacity at equilibrium, C_e (mg/L) is the equilibrium concentration of the solution, R (8.314 J/mol K) is the gas constant, T (K) is the absolute temperature and K_d (L/g) is the Langmuir constant.

The value of $\Delta G° < 0$, $\Delta H° > 0$ indicated the adsorption of MB and MG is the spontaneous endothermic process. The $\Delta S° > 0$ indicated that the energy redistribution between MB (MG) and composites leads to the adsorption. It also reflects the affinity with the adsorbent for the adsorbate mainly based on electrostatic interactions.

3.6. Stability of nZVI/MWCNTs/APT and removal of other dyes

Because the pure nZVI is oxidized in the air to reduce its reactivity will limit nZVI wide application. The stability of nZVI and nZVI/MWCNTs/APT were studied and the result is shown in Fig. 6a. It can be observed that nZVI/MWCNTs/APT composites have higher degradation activity for MB

Table 3
Adsorption isotherms parameters in binary-dye solutions

	Model	Parameters	Temperature (K)			SD
			303	313	323	
MB	Langmuir	q_m	147.3	147.5	149.9	
		b	0.3574	0.3758	0.4286	
		R^2	0.9957	0.9907	0.9914	0.0022
	Freundlich	K	59.7	62.9	64.3	
		$1/n$	0.1977	0.2161	0.2133	
		R^2	0.8156	0.9639	0.9831	0.0748
	Temkin	β	20.99	21.37	20.40	
		k_T	13.52	13.66	20.91	
		R^2	0.8785	0.9424	0.9586	0.0346
MG	Langmuir	q_m	138.3	148.4	177.9	
		b	0.4023	1.2669	3.6257	
		R^2	0.9518	0.8835	0.9624	0.0370
	Freundlich	K	59.4	50.8	118.0	
		$1/n$	0.2810	0.1883	0.1749	
		R^2	0.8902	0.8366	0.9316	0.0389
	Temkin	β	24.02	18.34	19.37	
		k_T	9.56	153.92	677.27	
		R^2	0.8183	0.7469	0.9097	0.0666

Table 4
Adsorption capacities of various adsorbents for MB and MG

	Adsorbent	q_m (mg/g)	Adsorption time (min)	Reference
MB	nZVI/MWCNTs/APT	149.9	90	This paper
	G–CNT	81.97	200	[41]
	MWCNT	59.7	160	[21]
	nZVI	112.8	–	[42]
	RM@C	76.92	180	[43]
MG	nZVI/MWCNTs/APT	177.9	90	This paper
	MWCNTs-COOH	49.45	120	[44]
	HNTs	99.6	120	[45]
	Fe^0-AC	100.12	80	[46]

and MG than nZVI from the beginning. After 45 d exposed in air, the removal efficiencies of MB and MG by using nZVI/MWCNTs/APT are still above 80%. It further illustrated that supporters MWCNTs/APT could not only as a dispersant to prevent nZVI from aggregation but also as a stabilizer to protect nZVI from the oxidation by air.

In order to investigate the removal ability of nZVI/MWCNTs/APT for other dyes (such as cationic dyes CV, BF and RhB and anionic dyes NGB, AYR, Orange IV and MO) batch experiments were performed after reaction 90min. The removal efficiencies are shown in Fig. 6b. Obviously, the removal efficiency of nZVI/MWCNTs/APT for cationic dyes CV and BF is greater than anionic. This is because the nZVI/MWCNTs/APT composite possesses a negatively charged surface in the wide range pH according to zeta potential for nZVI/MWCNTs/APT (Fig. 4b) that suggest there is a strong electrostatic attraction between nZVI/MWCNTs/APT and cationic dyes. Thus, electrostatic attraction plays an important role in cationic dye removal. However, the cationic dye RB doesn't present desirable removal efficiency. This may be related to the structure of dye molecular. BF and CV have belonged to planar molecular that removal performance greater than RB with a non-planar structure [47]. Therefore, the structure of dye molecules exerts a certain influence on the removal process. To sum up, it is speculated that the removal mechanism of cationic dyes using nZVI/MWCNTs/APT is based on simultaneous or consecutive adsorption and reduction reaction.

3.7. The reusability of nZVI/MWCNTs/APT

Many adsorbents were discarded after removing pollutants to re-contaminates the environment due to a release of pollutants again. Since MWCNTs have a unique structure to

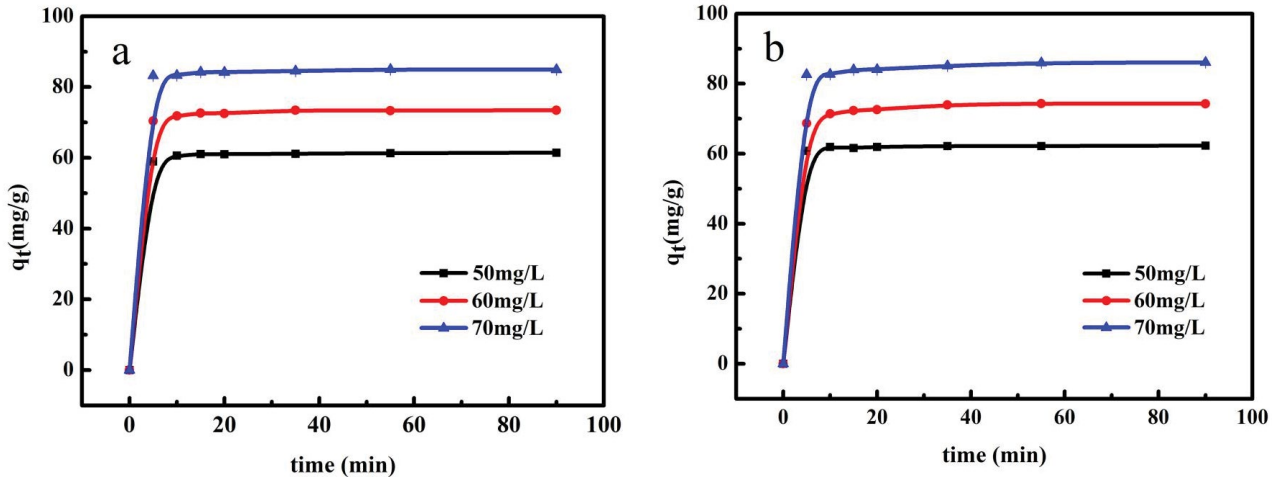

Fig. 5. Effect of contact time on the removal of MB and MG in binary systems. (Dosage = 0.08 g; solution volume = 100 mL; t = 0–90 min).

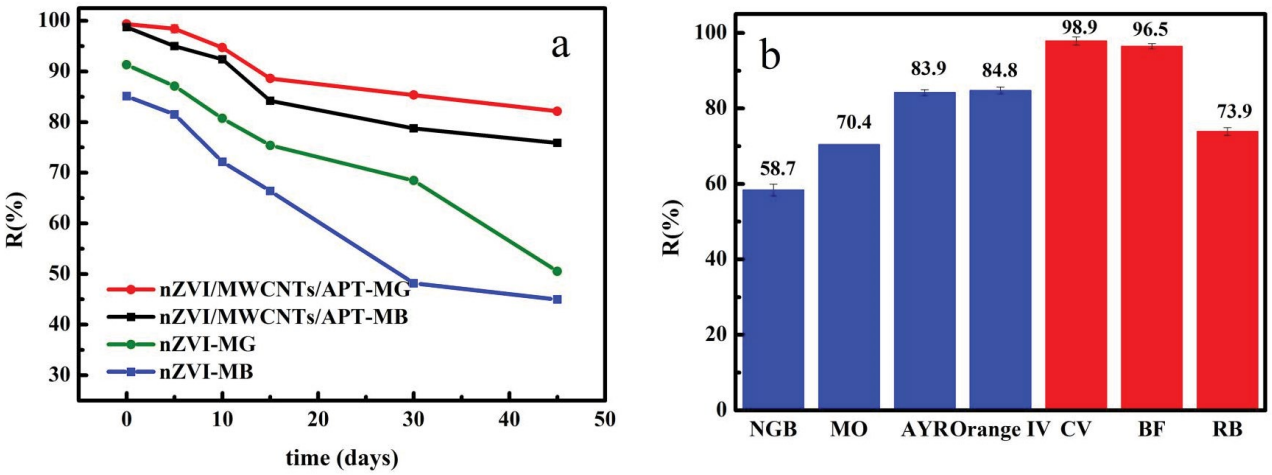

Fig. 6. Stability of nZVI/MWCNTs/APT and removal of other dyes.

use as electrode materials. Also, most organic dyes have a large amount of unsaturated chromophore groups and aromatic ring conjugated systems and make them pose definite electroactivity. When the electroactive dyes adsorbed on the nZVI/MWCNTs/APT surface was beneficial to improve adsorbent electrochemical performance. Therefore, reuse the waste nZVI/MWCNTs/APT that removal MB and MG from sewage to measure its electrochemical properties in Fig. S2. The purpose of the study is to explore the possibility of reusing them after adsorption rather than being discarded. The cyclic voltammetry curve (CV) results show that the curve before adsorption is close to the rectangular shape (Fig. S2a), indicating nZVI/MWCNTs/APT has good capacitance characteristics. After adsorption of the dye, there was an obvious symmetrical reversible redox peaks and the oxidation and reduction potential were 0.22 and 0.11 V, which means the existence of faraday reaction related to MB and MG as well as degradation intermediates. The specific capacitance is respectively 20.7 and 77 F/g at the current density of 1 A/g before and after adsorption of dyes by calculation of charge-discharge curves (Fig. S2b). The increase of the specific capacitance was mainly the electrochemical activity of dyes. Fig. S2c shows the impedance changes in the material. It is found the radius of the high-frequency region of the electrode material after adsorption dyes are comparatively small and the linear slope of the

Table 5
Thermodynamic parameters of MB and MG adsorption on nZVI/MWCNTs/APT

		T/K	$\Delta G°$/KJ mol^{-1}	$\Delta H°$/^{KJ} mol^{-1}	$\Delta S°$/J(^{mol} K)$^{-1}$
Binary dye	MB	303	–3.34	0.24	11.79
		313	–3.44		
		323	–3.57		
	MG	303	–4.91	54.14	194.51
		313	–6.49		
		323	–8.82		

low-frequency region is larger to indicate the used nZVI/MWCNTs/APT materials have the lower electron transfer impedance and better conductivity. Hence, the electro performance of nZVI/MWCNTs/APT after adsorbed dyes indicated it can be used as an electrode of supercapacitors instead of being discarded.

3.8. Adsorption and degradation mechanism

3.8.1. Analysis and identification of degradation products using GC-MS

In order to verify the degradation reaction to MB and MG were main the role of nZVI/MWCNTs/APT, this study first analyzed the degradation intermediates of MB and MG by GC-MS can identify slight organic matter after dye degradation. Many different m/z fragments (in the Fig. S5) appear in the mass spectrum is helpful to identify the degradation intermediate formation of MB and MG and confirm the oxidative degradation properties of the nZVI surface.

The degradation pathway of MB and MG was further analyzed as shown in Fig. S3 and S4 . In the nZVI/MWCNTs/APT system, MWCNTs/APT carriers can accelerate the mass transfer rate of MB and MG to make the dye molecules easily diffuse to the adsorbent surface active sites. Then, nZVI is oxidized to generate electrons and the dye molecules receive electrons to destroy decolorizing groups of MB (MG) then gradually decomposed into transition compounds. The amount of H^+ augment as the OH^- is consumed in the reaction of unstable transition compounds broken down into small molecules and accompanied degradation of chromospheres and conjugated systems. Based on the GC-MS spectrum, it is speculated that the MB main degradation pathway oxidizes C–S^+=C and C–N=C by addition reaction to form of intermediates from m/z = 354 to 322, 203, 178, 161, 122, and 91. The peak of m/z = 203 indicated that phenothiazine is oxidized to make C=C and C=S^+ cleavaged under H^+ exists conditions, resulting in phenothiazine heterocyclic opening at the center of its structure. The 2,5-diamino-4-methylbenzenesulfonic acid has been easily hydrolyzed rearrangement under H^+ exists conditions and finally decomposed into benzene sulfonic acid and carboxylic acid at the peak of m/z = 161 and m/z = 91, respectively. MG is a triphenylmethane dye and its possible degradation pathway is also speculated. The peaks from m/z = 354 to 291, 263, 135, 122, 117,103, 99, 73, and 59 appeared in Fig. 7 that –C=C– was oxidized through hydrogenation reaction. Briefly, the peak of m/z = 354 showed MG accepts an electron to happen N-demethylation and the peak of m/z = 291 occurs hydroxylation addition reaction to generate 4,4-bis(dimethylamino) benzophenone at m/z = 263.

The 4,4-bis(dimethylamino) benzophenone was oxidized to benzoic acid at m/z = 122, then possibly have two decompose products 3-hydroxybutyric acid and 4-hydroxy-4methyl-2-pentanone, and they will further hydrolyze and rearrange to produce acetic acid. It concludes of the above analysis the MB and MG transformed into less toxic acid metabolites in the nZVI/MWCNTs/APT system, illustrating the prepared nZVI/MWCNTs/APT nanocomposites has certain application prospects of dealing with environmental sewage.

3.8.2. The curve of UV-Vis absorbance of MB and MG decolorization

The transformation was explained that molecular characteristics and structure were clarified in the decolorization process by analyzing the ultraviolet-visible absorption spectra and in a color change of dye. As described in Fig. 7a, MB and MG exhibit two absorption peaks in the UV-vis spectrum and the absorbance at 292 and 248 nm are related to the aromatic ring. The maximum absorption wavelength of MB and MG at 664 and 617 nm belong to the functional group of –C=N– and –C=C–, respectively [48]. The intensity of the visible band closely related to the decolorization of MB and MG gradually decreases with the reaction time increase, which indicates that –C=N–, –C=C– the band of MB and MG are destroyed by nZVI [48]. The result is also confirmed by the change in the color of the dye in Fig. 7b. Based on the results of GC-MS and UV-vis spectra, the removal interaction of MB and MG by nZVI/MWCNTs/APT can be described in Fig. 7c. The process of degradation of MG and MB by nZVI/MWCNTs/APT involves simultaneous adsorption and reduction. On the one hand, MB and MG are adsorbed on the surface of nZVI/MWCNTs/APT by electrostatic attraction, π–π interaction and hydrogen bonding; on the other hand, the MB and MG are degraded by nZVI and simultaneously that transformed into the small fragments molecular access the solution.

4. Conclusion

In summary, nZVI/MWCNTs/APT nanocomposites were prepared through liquid-phase reduction. Among them, MWCNTs/APT as composite supporter materials not only improved the reactivity and stability of nZVI but also enhanced the adsorption performance of dyes. The results showed that nZVI/MWCNTs/APT exhibited high removal performance of cationic dyes compared to anionic dyes. Additionally, the structures of dyes' molecules exerted a certain influence on the removal process. The maximum adsorption capacity for cationic dyes MB and MG was 149.9 and 177.9 mg/g in binary system, indicating that it was a high removal performance. The thermodynamic parameters confirmed that the removal process was an endothermic, entropy increase and spontaneous process. Adsorption isotherm and kinetics were described that it fitted well with Langmuir adsorption isotherm and the PSO model. Removal mechanism suggested that adsorption and reduction were both involved in the removal process, and high removal efficiencies of cationic dyes were mainly attributed to the adsorption process induced by electrostatic, hydrogen bonding and π–π interactions. Consequently, the degradation of dyes solutions caused decoloration, and an appreciable degree of destruction in the dye molecule. The intermediate's structure was detected by using the GC-MS technique. Another important conclusion was that the waste adsorbent had a certain specific capacitance and can be used for the electrode materials of supercapacitors, which provided a new path for the recycling of materials. Overall, this study strongly indicated that the nZVI/MWCNTs/APT as a low-cost and eco-friendly material could be potentially used for the practical simultaneous removal of organic dyes.

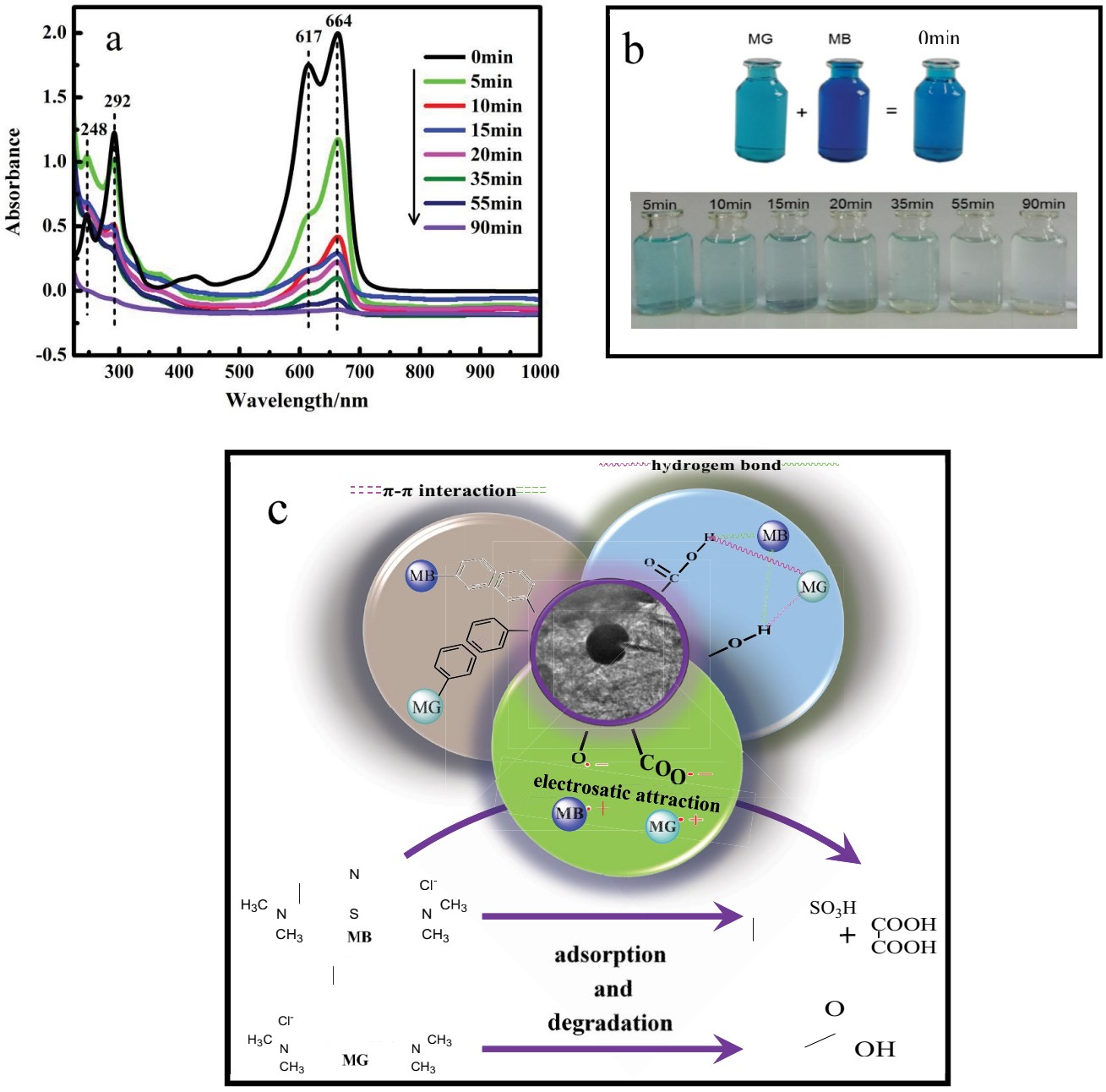

Fig. 7. nZVI/MWCNTs/APT removal MB and MG of (a) color changes, (b) variation of UV-Vis spectra and, (c) interaction and possible products of degradation.

Acknowledgement

This work was supported by the National Natural Science Foundation of China (NSFC) (51763015, 51503092), the Program for Hongliu First-class Discipline Construction in Lanzhou University of Technology.

References

[1] K.B. Tan, M. Vakili, B.A. Horri, P.E. Poh, A.Z. Abdullah, B. Salamatinia, Adsorption of dyes by nanomaterials: Recent developments and adsorption mechanisms, Sep. Purif. Technol., 150 (2015) 229–242.

[2] K.V.G. Ravikumar, S. Santhosh, S.V. Sudakaran, Y.V. Nancharaiah, P. Mrudula, N. Chandrasekaran, A. Mukherjee, Biogenic nano zero-valent iron (Bio-nZVI) anaerobic granules for textile dye removal, J. Environ. Chem. Eng., 6 (2018) 1683–1689.

[3] Mu. Naushad, A.A. Alqadami, Z.A. AlOthman, I.H. Alsohaimi, M.S. Algamdi, A.M. Aldawsari, Adsorption kinetics, isotherm and reusability studies for the removal of cationic dye from aqueous medium using arginine modified activated carbon, J. Mol. Liq., 293 (2019) 111442.

[4] A.A. Alqadami, Mu. Naushad, Z.A. Alothman, T. Ahamad, Adsorptive performance of MOF nanocomposite for methylene blue and malachite green dyes: kinetics, isotherm and mechanism, J. Environ. Manage., 223 (2018) 29–36.

[5] C.H.C. Tan, S. Sabar, M.H. Hussin, Development of immobilized microcrystalline cellulose as an effective adsorbent for methylene blue dye removal, S. Afr. J. Chem. Eng., 26 (2018) 11–24.
[6] S. Dutta, R. Saha, H. Kalita, A.N. Bezbaruah, Rapid reductive degradation of azo and anthraquinone dyes by nanoscale zero-valent iron, Environ. Technol. Innovation, 5 (2016) 176–187.
[7] Mu. Naushad, G. Sharma, Z.A. Alothman, Photodegradation of toxic dye using Gum Arabic-crosslinked poly(acrylamide)/$Ni(OH)_2$/FeOOH nanocomposites hydrogel, J. Cleaner Prod., 241 (2019) 118263.
[8] S.S. Wang, M.Y. Zhao, M. Zhou, Y.C. Li, J. Wang, B. Gao, S. Sato, K. Feng, W. Yin, A.D. Igalavithana, P. Oleszczuk, X. Wang, Y.S. Ok, Biochar-supported nZVI (nZVI/BC) for contaminant removal from soil and water: a critical review, J. Hazard. Mater., 373 (2019) 820–834.
[9] A. Babuponnusami, K. Muthukumar, A review on Fenton and improvements to the Fenton process for wastewater treatment, J. Environ. Chem. Eng., 2 (2014) 557–572.
[10] X. Wang, J. Yang, M. Zhu, Effects of PMMA/anisole hybrid coatings on discoloration performance of nano zerovalent iron toward organic dyes, J. Taiwan Inst. Chem. Eng., 45 (2014) 937–946.
[11] F. Zhu, S. He, T. Liu, Effect of pH, temperature and co-existing anions on the removal of Cr(VI) in groundwater by green synthesized nZVI/Ni, Ecotoxicol. Environ. Saf., 163 (2018) 544–550.
[12] Y. Chen, Z.H. Lin, R.R. Hao, H. Xu, C. Huang, Rapid adsorption and reductive degradation of Naphthol Green B from aqueous solution by Polypyrrole/Attapulgite composites supported nanoscale zero-valent iron, J. Hazard. Mater., 371 (2019) 8–17.
[13] A.A. Alqadami, Mu. Naushad, Z.A. Alothman, A.A. Ghfar, Novel metal–organic framework (MOF) based composite material for the sequestration of U(VI) and Th(IV) metal ions from aqueous environment, ACS Appl. Mater. Interfaces, 9 (2017) 36026–36037.
[14] B. Mu, A.Q. Wang, Adsorption of dyes onto palygorskite and its composites: s review, J. Environ. Chem. Eng., 4 (2016) 1274–1294.
[15] Y. Zheng, A.Q. Wang, Superadsorbent with three-dimensional networks: from bulk hydrogel to granular hydrogel, Eur. Polym. J., 72 (2015) 661–686.
[16] H. Xu, Y.J. Zhang, Y. Cheng, W. Tian, Z. Zhao, J. Tang, Polyaniline/attapulgite-supported nanoscale zero-valent iron for the rival removal of azo dyes in aqueous solution, Adsorpt. Sci. Technol., 37 (2019) 217–235.
[17] C.L. Li, H. Xu, J.L. Zhang, W. Wang, J. Tang, J.X. Wu, Improved study on the performance of polyacrylamide/attapulgite clay composite material-removing copper (II) ions from aqueous solution, Key Eng. Mater., 609–610 (2014) 26–31.
[18] I.H. Alsohaimi, M.A. Khan, Z.A. Alothman, M.R. Khan, M. Kumar, A.M. Al Mahri, Synthesis, characterization, and application of Fe-CNTs nanocomposite for BrO_3^- remediation from water samples, J. Ind. Eng. Chem., 26 (2015) 218–225.
[19] B. Sarkar, S. Mandal, Y.F. Tsang, P. Kumar, K.-H. Kim, Y.S. Ok, Designer carbon nanotubes for contaminant removal in water and wastewater: a critical review, Sci. Total Environ., 612 (2018) 561–581.
[20] J. Xu, Z. Cao, Y. Zhang, Z. Yuan, Z. Lou, X. Xu, X. Wang, A review of functionalized carbon nanotubes and graphene for heavy metal adsorption from water: preparation, application, and mechanism, Chemosphere, 195 (2018) 351–364.
[21] S. Wang, C.W. Ng, W. Wang, Q. Li, Z. Hao, Synergistic and competitive adsorption of organic dyes on multiwalled carbon nanotubes, Chem. Eng. J., 197 (2012) 34–40.
[22] C.H. Chen, C.F. Chang, S.M. Liu, Partial degradation mechanisms of malachite green and methyl violet B by Shewanella decoloration is NTOU1 under anaerobic conditions, J. Hazard. Mater., 177 (2010) 281–289.
[23] M. Rajabi, B. Mirza, K. Mahanpoor, M. Mirjalili, F. Najafi, O. Moradi, H. Sadegh, R. Shahryari-ghoshekandi, M. Asif, I. Tyagi, S. Agarwal, V.K. Gupta, Adsorption of malachite green from aqueous solution by carboxylate group functionalized multi-walled carbon nanotubes: determination of equilibrium and kinetics parameters, J. Ind. Eng. Chem., 34 (2016) 130–138.
[24] A. Xue, S. Zhou, Y. Zhao, X. Lu, P. Han, Effective NH_2-grafting on attapulgite surfaces for adsorption of reactive dyes, J. Hazard. Mater., 194 (2011) 7–14.
[25] J. Zhang, Q. Wang, A. Wang, Synthesis and characterization of chitosan-g-poly (acrylic acid)/attapulgite superabsorbent composites, Carbohydr. Polym., 68 (2007) 367–374.
[26] L. Leng, X. Yuan, G. Zeng, el at., Surface characterization of rice husk bio-char produced by liquefaction and application for cationic dye (Malachite green) adsorption, Fuel, 155 (2015) 77–85.
[27] G. Sheng, A. Alsaedi, W. Shammakh, S. Monaquel, J. Sheng, X. Wang, H. Li, Y. Huang, Enhanced sequestration of selenite in water by nanoscale zero-valent iron immobilization on carbon nanotubes by a combined batch, XPS and XAFS investigation, Carbon, 99 (2016) 123–130.
[28] H. Xu, W.G. Tian, Y.J. Zhang, J. Tang, Z. Zhao, Y. Chen, Reduced graphene oxide/attapulgite-supported nanoscale zero-valent iron removal of Acid Red 18 from aqueous solution, Water Air Soil Pollut., 299 (2018) 388.
[29] T. Wang, J. Su, X. Jin, Z. Chen, M. Megharaj, R. Naidu, Functional clay supported bimetallic nZVI/Pd nanoparticles used for removal of methyl orange from aqueous solution, J. Hazard. Mater., 262 (2013) 819–825.
[30] G. Quan, J. Zhang, J. Guo, Y. Lan, Removal of Cr(VI) from aqueous solution by nanoscale zero-valent iron grafted on acid-activated attapulgite, Water Air Soil Pollut., 225 (2014) 1979.
[31] I.M. Reck, R.M. Paixão , R. Bergamasco, M.F. Vieira, A.M.S. Vieira, Removal of tartrazine from aqueous solutions using adsorbents based on activated carbon and *Moringa oleifera* seeds, J. Cleaner Prod., 171 (2018) 85–97.
[32] A. Khodabandehloo, A. Rahbar-Kelishami, H. Shayesteh, Methylene blue removal using Salix babylonica (Weeping willow) leaves powder as a low-cost biosorbent in batch mode: kinetic, equilibrium, and thermodynamic studies, J. Mol. Liq., 244 (2017) 540–548.
[33] G. Crini, H.N. Peindy, F. Gimbert, C. Robert, Removal of C.I. basic Green 4 (Malachite Green) from aqueous solutions by adsorption using cyclodextrin-based adsorbent: kinetic and equilibrium studies, Sep. Purif. Technol., 53 (2007) 97–110.
[34] Md. A. Islam, I. Ali, S.M. Abdul Karim, Md. S.H. Firoz, Al-Nakib Chowdhury, D.W. Morton, M.J. Angove, Removal of dye from polluted water using novel nano manganese oxide-based materials, J. Water Process Eng., 32 (2019) 100911.
[35] M. Ghaedi, A. Hassanzadeh, S.N. Kokhdan, Multiwalled carbon nanotubes as adsorbents for the kinetic and equilibrium study of the removal of Alizarin Red S and Morin, J. Chem. Eng. Data, 56 (2011) 2511–2520.
[36] M.R. Sohrabi, N. Mansouriieh, M. Khosravi, M. Zolghadr, Removal of diazo dye Direct Red 23 from aqueous solution using zero-valent iron nanoparticles immobilized on multiwalled carbon nanotubes, Water Sci. Technol., 71 (2015) 1367–1374.
[37] M.L.F.A. De Castro, M.L.B. Abad, D.A.G. Sumalinog, R.R.M. Abarca, P. Paoprasert, M.D.G. de Luna, Adsorption of Methylene Blue dye and Cu(II) ions on EDTA-modified bentonite: isotherm, kinetic and thermodynamic studies, Sustainable Environ. Res., 28 (2018) 197–205.
[38] Y. Miyah, A. Lahrichi, M. Idrissi, A. Khalil, F. Zerrouq, Adsorption of methylene blue dye from aqueous solutions onto walnut shells powder: equilibrium and kinetic studies, Surf. Interfaces, 11 (2018) 74–81.
[39] N. Wang, J. Feng, J. Chen, J. Wang, W. Yan, Adsorption mechanism of phosphate by polyaniline/TiO_2 composite from wastewater, Chem. Eng. J., 316 (2017) 33–40.
[40] X. Liu, R. Wang, Z. Ni, W. Zhou, Y. Du, Z. Ye, R. Guo, Facile synthesis and selective adsorption properties of Sm_2CuO_4 for malachite green: kinetics, thermodynamics and DFT studies, J. Alloys Compd., 743 (2018) 17–25.
[41] L. Ai, J. Jiang, Removal of methylene blue from aqueous solution with self-assembled cylindrical graphene–carbon nanotube hybrid, Chem. Eng. J., 192 (2012) 156–163.

[42] R. Sawafta, T. Shahwan, A comparative study of the removal of methylene blue by iron nanoparticles from water and water-ethanol solutions, J. Mol. Liq., 273 (2019) 274–281.
[43] O. Kazak, Y.R. Eker, I. Akin, H. Bingol, A. Tor, A novel red mud@ sucrose based carbon composite: preparation, characterization and its adsorption performance toward methylene blue in aqueous solution, J. Environ. Chem. Eng., 5 (2017) 2639–2647.
[44] H. Sadegh, R. Shahryari-ghoshekandi, S. Agarwal, I. Tyagi, M. Asif, V.K. Gupta, Microwave-assisted removal of malachite green by carboxylate functionalized multi-walled carbon nanotubes: kinetics and equilibrium study, J. Mol. Liq., 206 (2015) 151–158.
[45] G. Kiani, M. Dostali, A. Rostami, A.R. Khatae, Adsorption studies on the removal of Malachite Green from aqueous solutions onto halloysite nanotubes, Appl. Clay Sci., 54 (2011) 34–39.
[46] P. Singh, P. Raizada, S. Kumari, A. Kumar, D. Pathania, P. Thakur, Solar-fenton removal of malachite green with novel Fe^0-activated carbon nanocomposite, Appl. Catal., A, 476 (2014) 9–18.
[47] C.-H. Liu, J.-J. Li, H.-L. Zhang, B.-R. Li, Y. Guo, Structure dependent interaction between organic dyes and carbon nanotubes, Colloids Surf., A, 313 (2008) 9–12.
[48] X. Wang, A. Wang, J. Ma, M. Fu, Facile green synthesis of functional nanoscale zero-valent iron and studies of its activity toward ultrasound-enhanced decolorization of cationic dyes, Chemosphere, 166 (2017) 80–88.

Supplementary information

Simultaneous removal of binary cationic dyes from wastewater by nanoscale zero-valent iron particles supported on multiwalled carbon nanotubes/attapulgite.

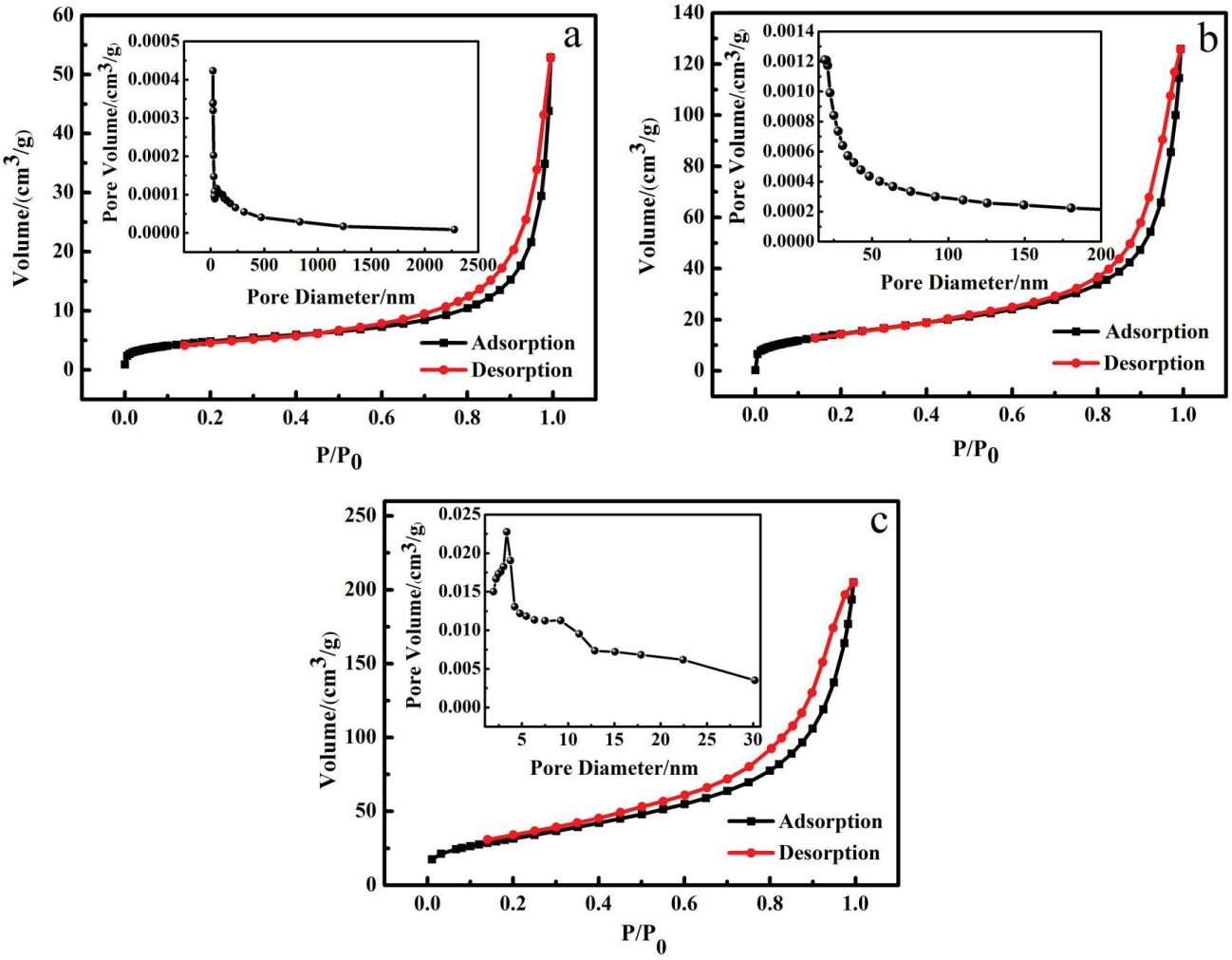

Fig. S1. N_2 adsorption–desorption isotherms and pore size distribution of (a) nZVI and (b) and nZVI/MWCNTs/APT composite.

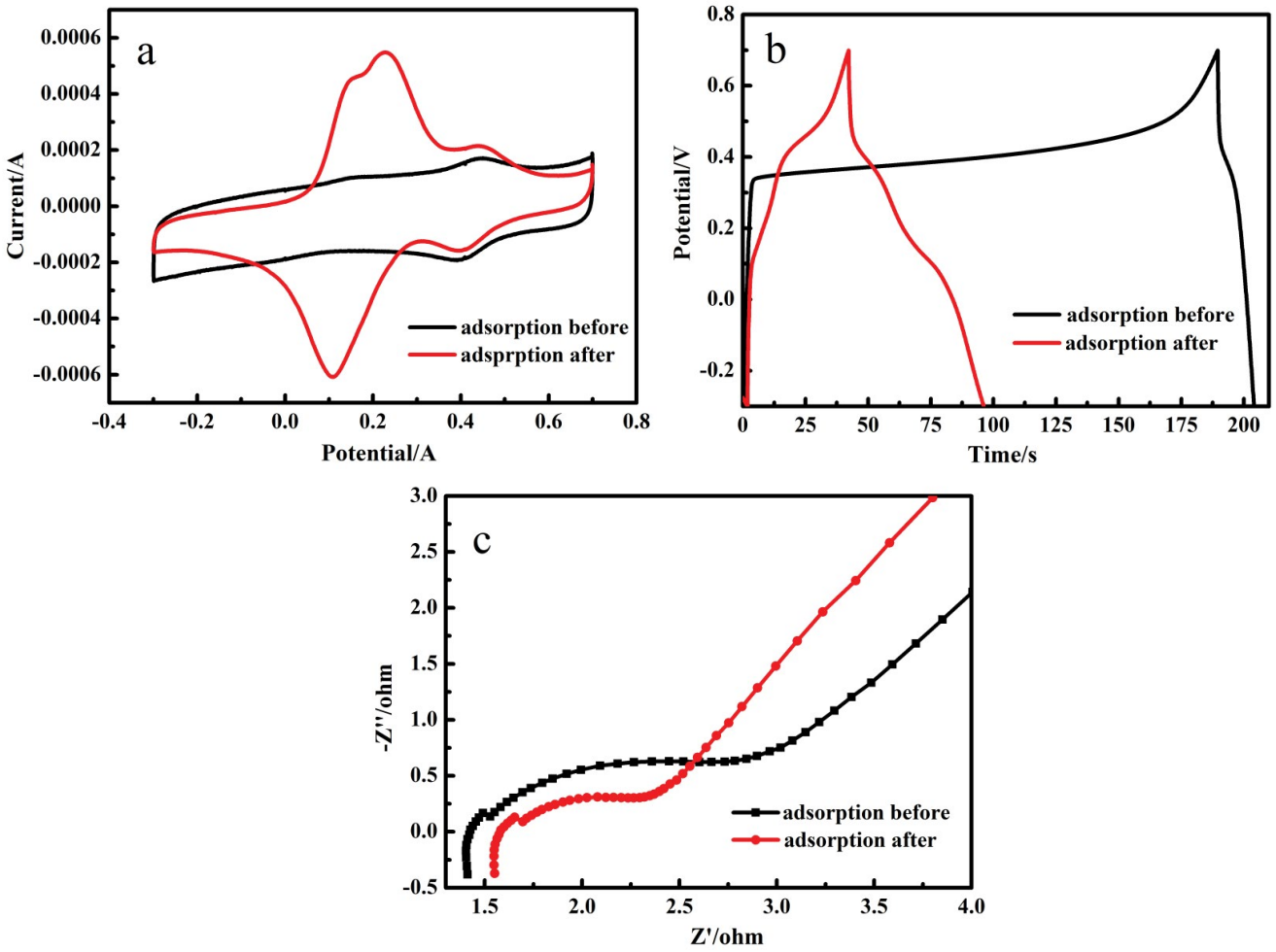

Fig. S2. Electrochemical properties of nZVI/MWCNTs/APT before and after removal of MB and MG: (a) CV curves, (b) charge-discharge curves, and (c) Electrochemical Impedance Spectroscopy (EIS).

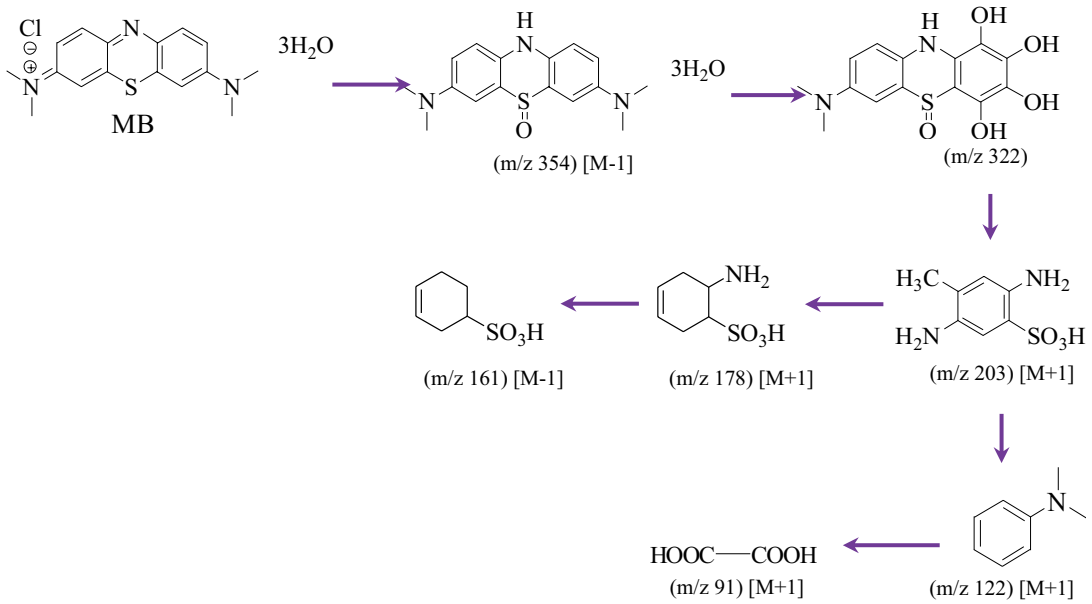

Fig. S3. Proposed degradation pathway of MB.

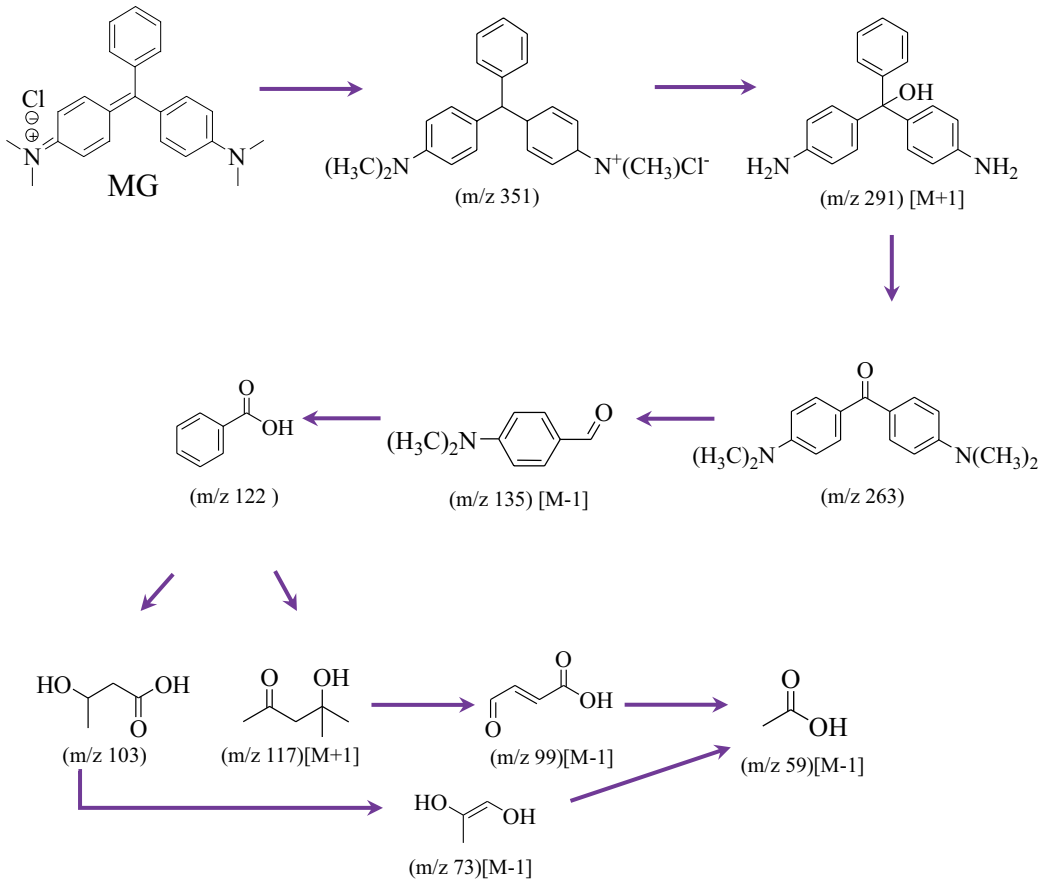

Fig. S4. Proposed degradation pathway of MG.

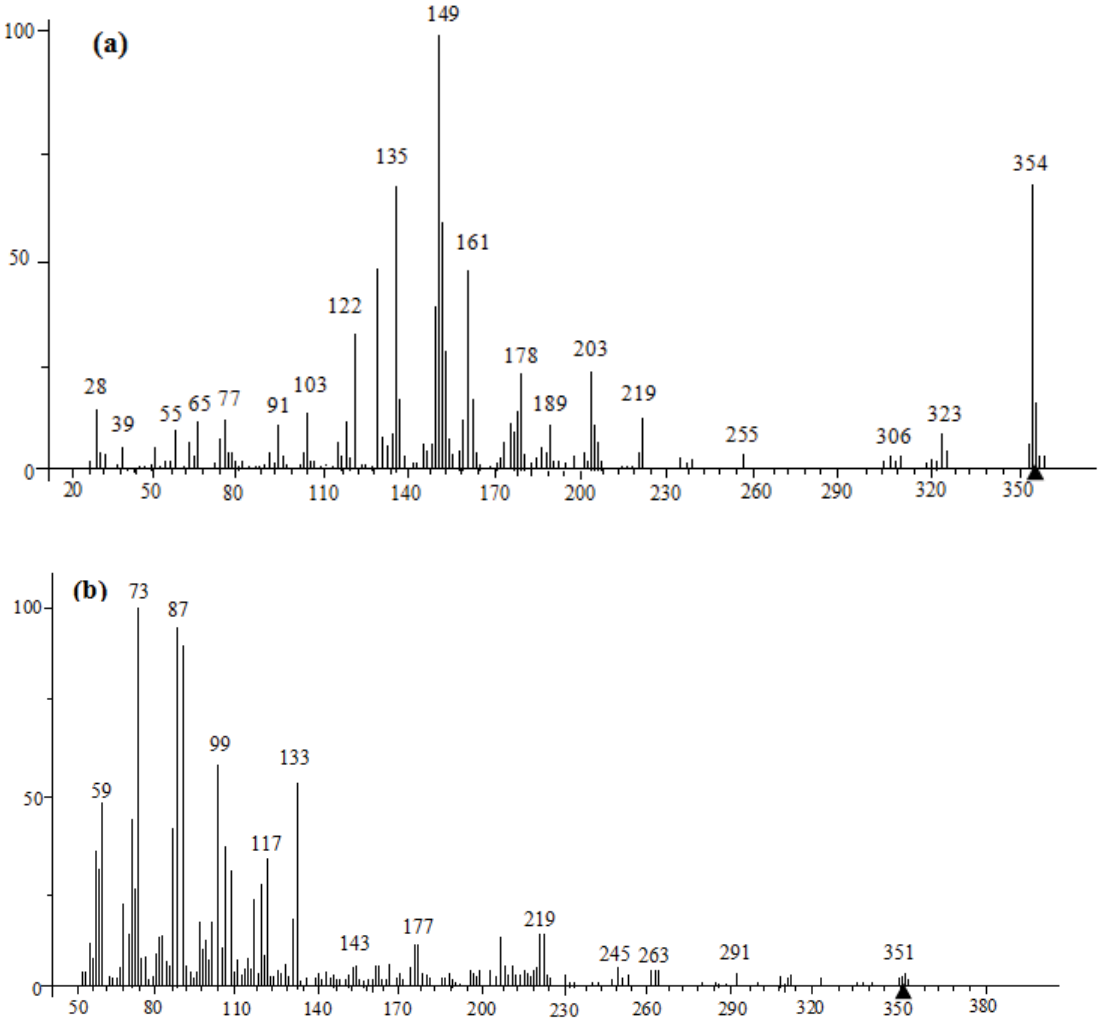

Fig. S5. GC-MS spectra of identified intermediates after degradation of MB and MG.